



Effect of chemical reaction and radiation absorption on MHD Casson fluid over an exponentially stretching sheet with slip conditions: ethanol as solvent

C. Arruna Nandhini^{1,a} , S. Jothimani¹ , Ali J. Chamkha² 

¹ Department of Mathematics, Government Arts College (Autonomous), Coimbatore, Tamil Nadu 641 018, India

² Faculty of Engineering, Kuwait College of Science and Technology, 35004 Doha District, Kuwait

Received: 12 September 2022 / Accepted: 3 January 2023

© The Author(s), under exclusive licence to Società Italiana di Fisica and Springer-Verlag GmbH Germany, part of Springer Nature 2023

Abstract A novel approach is devised to inspect the influence of universal solvent, ethyl alcohol, when mixed with Casson fluid across an exponentially stretching sheet, involving radiation absorption and chemical reaction. At the boundary, slip conditions are additionally considered. Utilizing appropriate similarity transformation, the governing partial differential equations are transfigured into a system of coupled ordinary differential equations. Subsequently, the resulting equations are solved numerically using MATLAB built-in technique `bvp4c`. Graphical results are presented for the gaseous and liquid state. The effect of pertinent parameters on the skin friction coefficient, heat and mass transfer rates are elucidated in tabular form. Furthermore, comparisons of the present results with previously published work show that the present results have high accuracy. It is noteworthy to mention that the combined effect of radiation absorption and slip conditions enhances the temperature distribution near the wall and suppresses it away from the wall in the case of Casson fluid blended with ethyl alcohol. Also, the effect of the chemical reaction parameter on the mass transfer rate is very influential. The present study is of immediate interest in biodiesel production, which serves as an attractive alternative to conventional petroleum diesel fuel.

1 Introduction

The inspection of non-Newtonian fluids past a stretching surface has recently achieved a great deal of attention owing to its diverse industrial applications and vital role in technological processes.

The precise solution for flow over a stretching sheet was developed primarily by Crane [1]. Among those found in the literature, Casson fluid is the most prominent non-Newtonian fluid. It was first coined by Casson [2] in 1959 during his research in the prognosis of the flow behaviour of printing ink suspended by pigment-oil. On the other hand, slip conditions have remarkable applications in manufacturing processes. Mukhopadhyay [3] examined the influence of partial slip parameters on MHD fluid flow over an exponentially stretching sheet incorporating suction or injection along with thermal radiation. Adopting slip conditions and an exponentially stretching sheet, Reddy et al. [4] explored the heat transfer rate of MHD Casson fluid flow. The majority of researchers analysed the Casson fluid flowing across a stretching sheet.

With this in mind, many authors [5–7], and [8] have recently investigated the heat and mass transfer of Casson fluid with various geometries. Mousavi et al. [9] used the finite difference method to study MHD Casson hybrid nanofluid flow past a stretching or shrinking sheet, considering suction, radiation, and convective boundary condition effects. Hameed [10] studied the impact of Casson hybrid nanofluid with a magnetic field, heat generation, absorption, and viscous dissipation with couple stress flow on a nonlinear stretching surface analytically, and the Mathematica software was used to obtain the basic result.

From the scientific point of observation, the presence of radiation absorption makes the flow much more challenging. A typical paradigm of this is radiation absorption from neighbouring stars in planetary atmosphere. Shercliff [11] deliberated a viscous fluid flow that conducts electrically and is magnetically-induced with radiation absorption and mass transfer, which is fruitful in the field of planetary research.

Motivated by the aforementioned literature, this study seeks to unravel the impact of radiation absorption and slip conditions on MHD chemically reactive Casson fluid mixed with ethanol across an exponentially stretching sheet. A suitable similarity transformation is utilized to transmogrify the governing partial differential equations into coupled ordinary differential equations. MATLAB routine “`bvp4c`” was exerted to ascertain the numerical solution of the propounded problem.

^a e-mail: arruna98@gmail.com (corresponding author)

2 Mathematical formulation

Over an exponentially stretching sheet, a steady two-dimensional boundary layer slip flow of an incompressible viscous electrically conducting Casson fluid is examined. Further the consequences of chemical reactions and radiation absorption are additionally considered. By preserving the origin fixed, the stretching sheet is placed along the x -axis in the direction of the fluid motion and the y -axis is perpendicular to it. The flow dynamics occurs in the region $y > 0$ and is subjected to a magnetic field $B(x) = B_0 e^{\frac{x}{L}}$ is applied in the transverse direction, where B_0 is a constant. The stretching surface has $U = U_0 e^{\frac{x}{L}}$, $T_w = T_\infty + T_0 e^{\frac{x}{L}}$ and $C_w = C_\infty + C_0 e^{\frac{x}{L}}$. The physical model is depicted in Fig. 1.

Subject to the condition that the Casson fluid flow is in an isotropic and incompressible manner, the Casson fluid’s rheological equation can be written [12]

$$\tau_{ij} = \begin{cases} 2\left(\mu_B + \frac{p_y}{\sqrt{2\pi}}\right)e_{ij}, \pi > \pi_c \\ 2\left(\mu_B + \frac{p_y}{\sqrt{2\pi_c}}\right)e_{ij}, \pi < \pi_c \end{cases} \tag{1}$$

In the above equation, $\pi = e_{ij}e_{ij}$ and $p_y = \frac{\mu_B \sqrt{2\pi}}{\beta}$. According to the non-Newtonian paradigm, π_c is the critical value of π .

Employing the Boussinesq approximation whilst assuming the premise outlined above, the governing equations of flow in the usual notation are

$$\frac{\partial u}{\partial x} + \frac{\partial v}{\partial y} = 0, \tag{2}$$

$$u \frac{\partial u}{\partial x} + v \frac{\partial v}{\partial y} = \nu \left(1 + \frac{1}{\beta}\right) \frac{\partial^2 u}{\partial y^2} + g\beta_C(C - C_\infty) + g\beta_T(T - T_\infty) - \frac{\sigma B^2 u}{\rho}, \tag{3}$$

$$\rho c_p \left(u \frac{\partial T}{\partial x} + v \frac{\partial T}{\partial y}\right) = \kappa \frac{\partial^2 T}{\partial y^2} - \frac{\partial q_r}{\partial y} + \mu \left(1 + \frac{1}{\beta}\right) \left(\frac{\partial u}{\partial y}\right)^2 + \sigma B^2 u^2 + Q'(T - T_\infty) + Q^*(C - C_\infty), \tag{4}$$

$$u \frac{\partial C}{\partial x} + v \frac{\partial C}{\partial y} = D_m \frac{\partial^2 C}{\partial y^2} - k_l(C - C_\infty) \tag{5}$$

It is assumed that the heat source/sink takes the form $Q' = Q'_0 e^{\frac{x}{L}}$, radiation absorption is of the form $Q^* = Q_0^* e^{\frac{x}{L}}$ and the chemical reaction takes the following form $k_l = k_0 e^{\frac{x}{L}}$.

By utilizing the Rosseland approximation [13], the problem can be simplified and as a result q_r is defined as

$$q_r = -\frac{4\sigma^*}{3k^*} \frac{\partial T^4}{\partial y}. \tag{6}$$

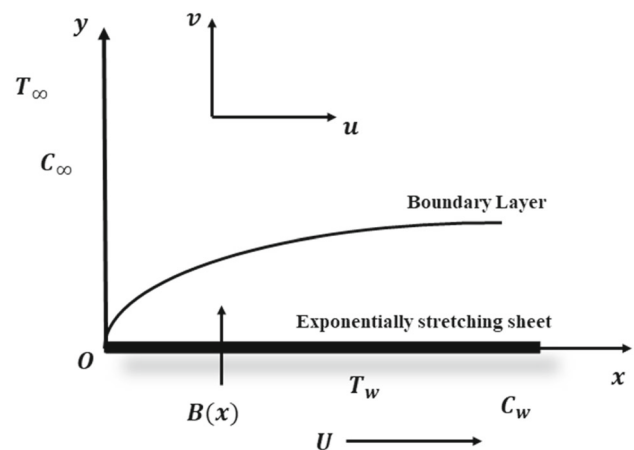
If the flow’s internal temperature variations are negligibly minimal, then a linear function of T_∞ can be used to express T^4 . When T^4 is expanded about T_∞ using Taylor’s series and subsequent truncation of higher order terms, we acquire

$$T^4 \equiv 4T_\infty^3 T - 3T_\infty^4.$$

Therefore, Eq. (4) becomes

$$\rho c_p \left(u \frac{\partial T}{\partial x} + v \frac{\partial T}{\partial y}\right) = \kappa \left(1 + \frac{16\sigma^* T_\infty^3}{3\kappa k^*}\right) \frac{\partial^2 T}{\partial y^2} + \mu \left(1 + \frac{1}{\beta}\right) \left(\frac{\partial u}{\partial y}\right)^2 + \sigma B^2 u^2 + Q'(T - T_\infty) + Q^*(C - C_\infty) \tag{7}$$

Fig. 1 Coordinate system of fluid flow



3 Boundary conditions

The apposite boundary constraints for the flow model are

$$\begin{aligned} \text{at } y = 0 : u = U + N_1 v \left(1 + \frac{1}{\beta} \right) \frac{\partial u}{\partial y}, v = -V(x), T = T_w + D_1 \frac{\partial T}{\partial y}, C = C_w + E_1 \frac{\partial C}{\partial y} \quad (8) \\ \text{as } y \rightarrow \infty, u \rightarrow 0, T \rightarrow T_\infty, C \rightarrow C_\infty. \quad (9) \end{aligned}$$

Here $N_1 = N_0 e^{-\frac{x}{2L}}$, $D_1 = D_0 e^{-\frac{x}{2L}}$ and $E_1 = E_0 e^{-\frac{x}{2L}}$. At the wall, an eccentric kind of velocity $V(x)$ is taken into consideration. In particular, $V(x) = V_0 e^{\frac{x}{2L}}$, where $V(x) > 0$ and $V(x) < 0$ signify the velocity of suction the velocity of bowing, respectively.

4 Method of solution

In order to simplify the analysis of the problem, a suitable similarity transformation is employed to convert the governing partial differential equations into nonlinear ordinary differential equations. The similarity variable ξ is introduced to satisfy the continuity Eq. (2) such that

$$u = U_0 e^{\frac{x}{2L}} f'(\xi), \quad (10a)$$

$$v = -\sqrt{\frac{vU_0}{2L}} e^{\frac{x}{2L}} \left[f(\xi) + \xi f'(\xi) \right], \quad (10b)$$

$$\text{where } \xi = \sqrt{\frac{U_0}{2vL}} e^{\frac{x}{2L}} y, \quad (10c)$$

$$T = T_\infty + T_0 e^{\frac{x}{2L}} \theta(\xi), \quad (10d)$$

$$C = C_\infty + C_0 e^{\frac{x}{2L}} \phi(\xi). \quad (10e)$$

Equations (3), (7) and (5) are transmogrified into the equivalent ordinary differential equations by employing the transformation stated above.

The transformed ordinary differential equations are

$$\left(1 + \frac{1}{\beta} \right) f'''' + f f'' - 2f'^2 - M f' + 2Gc\phi + 2Gr\theta = 0, \quad (11)$$

$$\frac{1}{Pr} \left(1 + \frac{4}{3}R \right) \theta'' + f\theta' - f'\theta + Q\theta + Ec \left(1 + \frac{1}{\beta} \right) f''^2 + M.Ec.f'^2 + Ra\phi = 0, \quad (12)$$

$$\phi'' - Sc(f'\phi - f\phi') - k.Sc\phi = 0, \quad (13)$$

The corresponding boundary constraints are articulated as follows:

$$\text{at } \xi = 0 : f(\xi) = s, f'(\xi) = 1 + S_v \left(1 + \frac{1}{\beta} \right) f''(0), \theta(\xi) = 1 + S_\theta \theta'(0), \phi(\xi) = 1 + S_\phi \phi'(0). \quad (14)$$

$$\text{as } \xi \rightarrow \infty : f'(\xi) \rightarrow 0, \theta(\xi) \rightarrow 0, \phi(\xi) \rightarrow 0. \quad (15)$$

where the prime notation symbolizes ξ – dependent differentiation.

The dimensionless parameters are

$$M = \frac{2\sigma B_0^2 L}{\rho U_0}, Gr = \frac{gL\beta_r(T_w - T_\infty)}{u^2}, Gc = \frac{gL\beta_c(C_w - C_\infty)}{u^2},$$

$$Pr = \frac{\mu c_p}{\kappa}, R = \frac{4\sigma^* T_\infty^3}{\kappa k^*}, Ec = \frac{U_0^2 e^{\frac{3x}{2L}}}{c_p T_0}, Q = \frac{2LQ'}{\rho c_p U_0}, Sc = \frac{v}{D_m}.$$

$$Ra = \frac{2Q_0^* C_0 L}{\rho c_p U_0 T_0}, k = \frac{2Lk_0}{U_0}, S_v = N_0 \sqrt{\frac{U_0 v}{2L}}, S_\theta = D_0 \sqrt{\frac{U_0}{2vL}},$$

$$S_\phi = E_0 \sqrt{\frac{U_0}{2vL}} \text{ and } s = \frac{V_0}{\sqrt{\frac{vU_0}{2L}}}.$$

In this flow problem, the physical quantities of concern are C_f , Nu_x and Sh_x . They are acquired as

$$\begin{aligned} \frac{C_f \sqrt{Re_x/2}}{\sqrt{x/L}} &= \left(1 + \frac{1}{\beta}\right) f''(0), \\ \frac{Nu_x}{\sqrt{Re_x/2} \sqrt{x/L}} &= -\theta'(0), \\ \frac{Sh_x}{\sqrt{Re_x/2} \sqrt{x/L}} &= -\phi'(0), \end{aligned}$$

where $Re_x = \frac{U_x v}{\nu}$. The aforementioned equations demonstrate that variations in C_f , Nu_x and Sh_x rely on the factors $\left(1 + \frac{1}{\beta}\right) f''(0)$, $-\theta'(0)$ and $-\phi'(0)$, respectively.

5 Results and discussion

In order to obtain the numerical solution, MATLAB bvp4c package [14] has been utilized to solve the resulting ordinary differential Eqs. (11) to (13) together with the relevant boundary constraints (14) and (15). This routine is a collocation method and implements the 3-stage Lobatto IIIa formula. Table 1 is presented to determine the reliability and precision of the numerical analysis that has been used. The numerical values of $-\theta'(0)$ for several values of Pr and R excluding other pertinent parameters are contrasted with the findings that are reported in the literature. The findings are well in line with the studies already available. For the sake of brevity, the outcomes are depicted by means of graphs and tables. Throughout this study, the dotted lines denote the slip flow for the case of ethyl alcohol (C_2H_5OH) at $25^\circ C$ with the default values of the associated parameters considered as $Pr = 18.05$, $Sc = 1.29$, $\beta = 2.5$, $R = k = s = Q = S_\theta = S_\phi = 0.2$, $S_v = M = 0.5$, $R_a = Ec = 0.1$, $Gr = G = 1$. On the other hand, the dashed lines denote the slip case with slip parameters chosen as $S_v = S_\phi = 0.5$ and $S_\theta = 0.1$ for the case of air with $Pr = Sc = 0.7$, $\beta = 2$, $Q = 0.2$, $M = s = R = Ec = 0.1$, $k = 0.5$ and $Gr = Gc = R_a = 1$. Similar values are chosen for the case of air with no-slip condition ($S_v = S_\theta = S_\phi = 0$) which are denoted using the solid lines.

Under limiting conditions, the framework of this present study is analysed for no-slip condition (solid lines) which are self-same with the extant findings in the literature.

The dominance of magnetic field parameter (M) on the velocity profile $f'(\xi)$, temperature distribution $\theta(\xi)$ and concentration distribution $\phi(\xi)$ are depicted in Figs. 2, 3 and 4, respectively. In the case of air, enhancement of M decreases the velocity profile due to Lorentz force. This consequence is attributed by virtue of introducing transverse magnetic field. In ethyl alcohol case, the velocity profile initially drops off close to the wall before rising farther away. When it comes to air, the temperature distribution gains in magnitude as M rises. But in the case of C_2H_5OH , similar pattern is witnessed as with velocity profile. A rise in the values of M increases the concentration distribution for both air and ethyl alcohol case.

For air, a rise in R increases both $f'(\xi)$ and $\theta(\xi)$. Moreover, for C_2H_5OH case, the velocity profile increases to some extent and then suppresses, but rises the temperature distribution. These are vividly noted in Figs. 5 and 6.

Figure 7 and 8 portray the striking effect of Q on $f'(\xi)$ and $\theta(\xi)$. Regarding the case of air, a boost in the values of Q enhances $f'(\xi)$. Intended for ethyl alcohol case, the velocity profile initially declines but shoots up away from the wall. Similar argument pertains to the temperature distribution.

It is witnessed from Figs. 9 and 10 that, when Eckert number (Ec) increases, in addition to $f'(\xi)$, $\theta(\xi)$ also increases for smaller values of Ec . On the contrary, for larger values of Ec , $f'(\xi)$ and $\theta(\xi)$ increases near the wall and suppresses suddenly.

Analogous results are obtained when radiation absorption (R_a) increases. These are seen distinctly through Figs. 11 and 12. Further it is well noted out of Fig. 13 that the concentration distribution depreciates as R_a increases.

Table 1 Correlation of present values of heat transfer coefficient $-\theta'(0)$ for changes in Pr and R

| Pr | R | Mukhopadhyay [3] | Pramanik [12] | Reddy et al. [4] | Present study |
|------|-----|------------------|---------------|------------------|---------------|
| 1 | 0 | 0.9547 | 0.9547 | 0.9548 | 0.954812 |
| 2 | | 1.4714 | 1.4714 | 1.4715 | 1.471454 |
| 3 | | 1.8691 | 1.8691 | 1.8691 | 1.869069 |
| 5 | | 2.5001 | 2.5001 | 2.5001 | 2.500125 |
| 10 | | 3.6603 | 3.6603 | 3.6605 | 3.660339 |
| 1 | 0.5 | | 0.6765 | 0.6775 | 0.677548 |
| | 1 | 0.5311 | 0.5315 | 0.5353 | 0.535303 |
| 2 | 0.5 | 1.0734 | 1.0734 | 1.0735 | 1.073517 |
| | 1 | 0.8626 | 0.8626 | 0.8629 | 0.862888 |
| 3 | 0.5 | 1.3807 | 1.3807 | 1.3807 | 1.380746 |
| | 1 | 1.1213 | 1.1213 | 1.1214 | 1.121422 |

Fig. 2 Velocity profile for various M

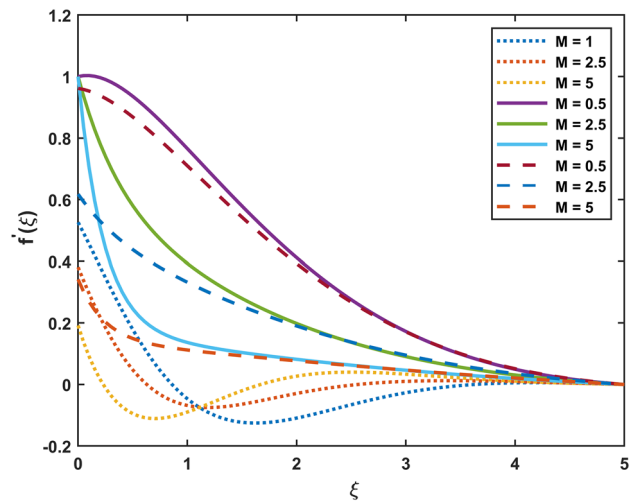


Fig. 3 Temperature distribution for various M

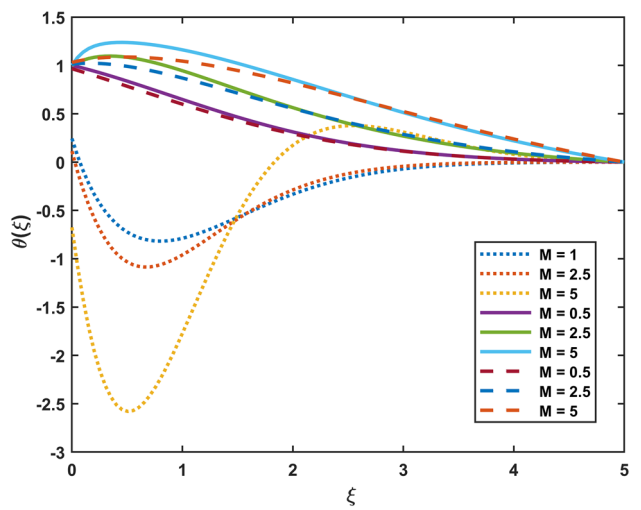
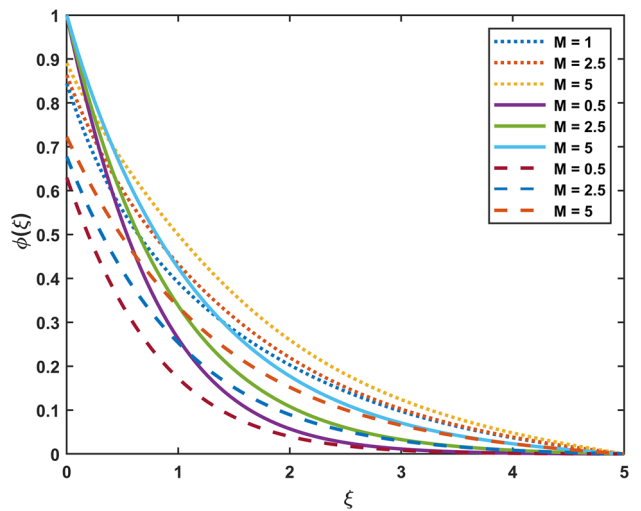


Fig. 4 Concentration distribution for various M



From Figs. 14 and 15, it becomes apparent that enhancement of k depreciates the velocity profile and temperature distribution for air, but for ethyl alcohol the trend gets reversed away from the wall. A rise in the values of k declines the concentration distribution for both air and ethyl alcohol (Fig. 16).

The results in Figs. 17, 18 and 19 demonstrate that, for both the gaseous and liquid state, the efficacy of increasing s decreases the velocity profile. Identically temperature and concentration distributions also get declined.

Fig. 5 Velocity profile for various R

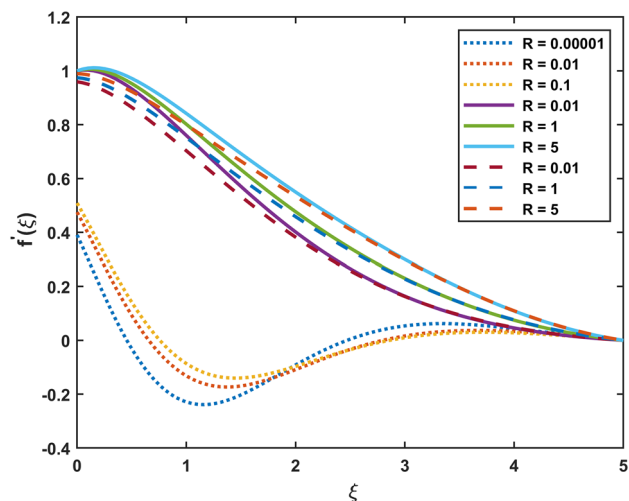


Fig. 6 Temperature distribution for various R

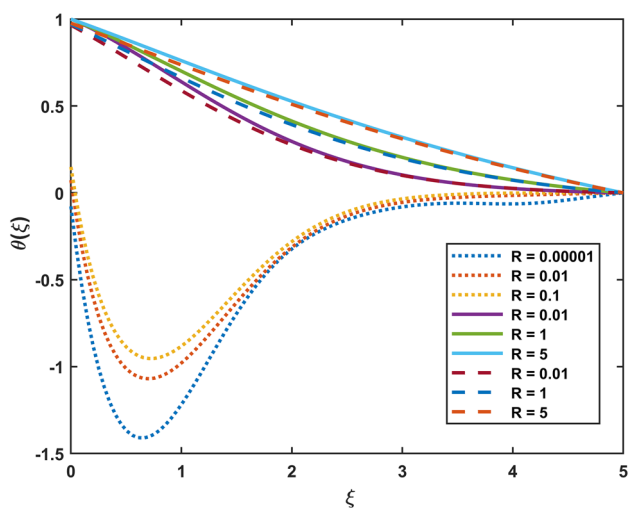
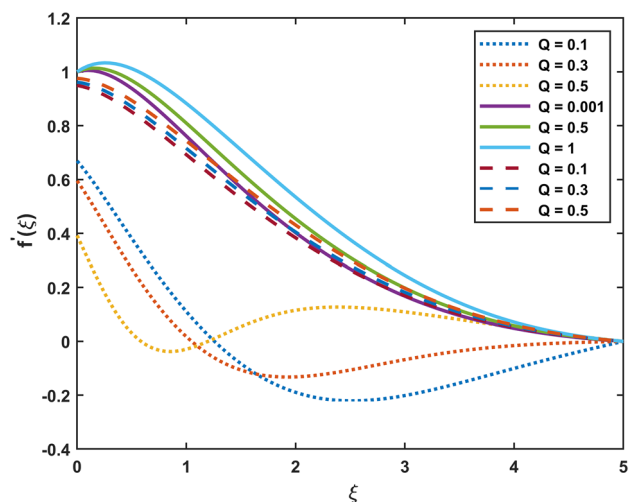


Fig. 7 Velocity profile for various Q



For both cases under consideration, proliferating S_v suppresses the velocity profile and temperature distribution, whilst the concentration distribution skyrockets. These are presented in Figs. 20, 21 and 22.

As thermal slip parameter (S_θ) increases, $\theta(\xi)$ as well as $f'(\xi)$ decreases, but the concentration distribution increases for air. However, this is not the trend for the case of ethyl alcohol (Figs. 23, 24, and 25).

Fig. 8 Temperature distribution for various Q

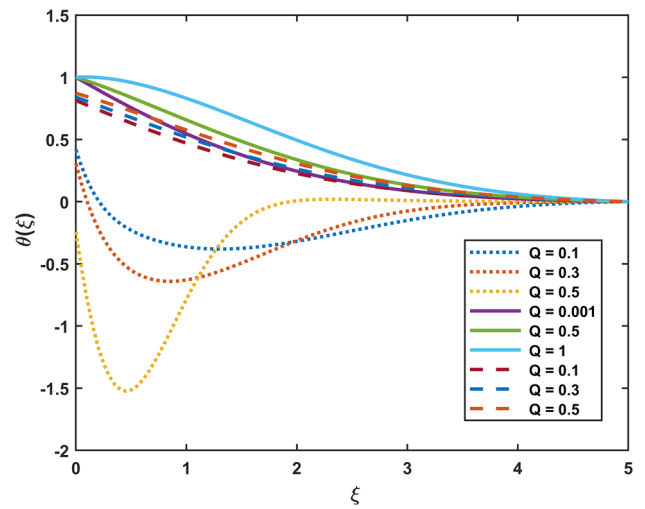


Fig. 9 Velocity profile for various Ec

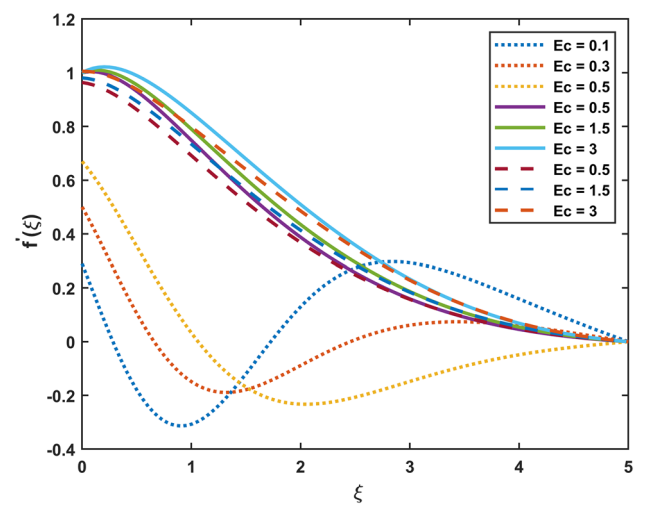
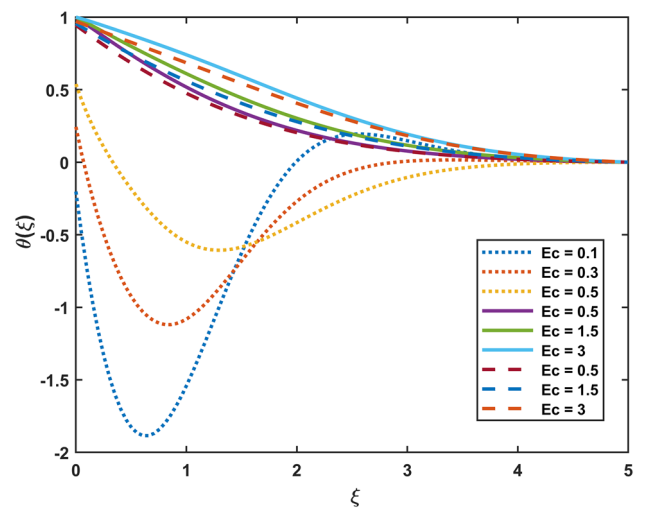


Fig. 10 Temperature distribution for various Ec



The behaviour of solutal slip (S_ϕ) is illustrated in Figs. 26, 27 and 28. For both air and ethyl alcohol, enhancement of S_ϕ reduces the velocity profile. Similarly, the temperature and concentration distributions get suppressed.

Figures 29, 30, and 31 reveal the impingement of Casson fluid parameter (β) on $f'(\xi)$, $\theta(\xi)$ and $\phi(\xi)$, respectively. As β augments, the temperature intensifies which in turn suppresses the velocity profile and concentration distribution for air. Similar trend is reflected in the case of ethyl alcohol.

Fig. 11 Velocity profile for various R_a

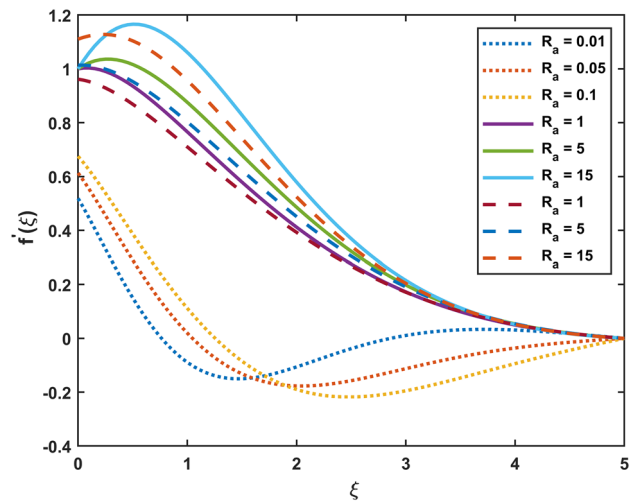


Fig. 12 Temperature distribution for various R_a

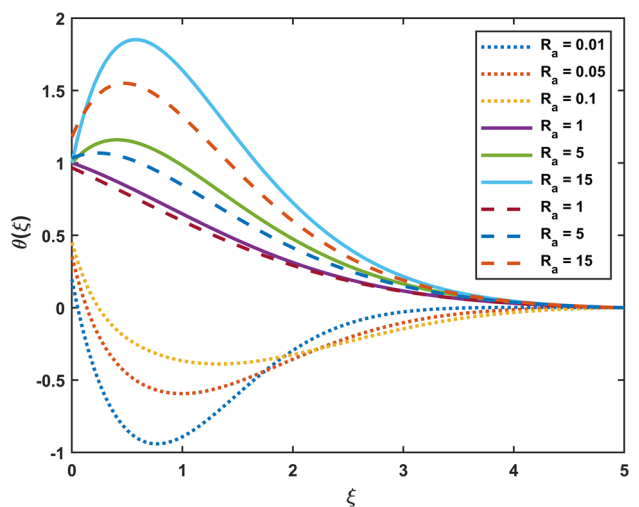


Fig. 13 Concentration distribution for various R_a

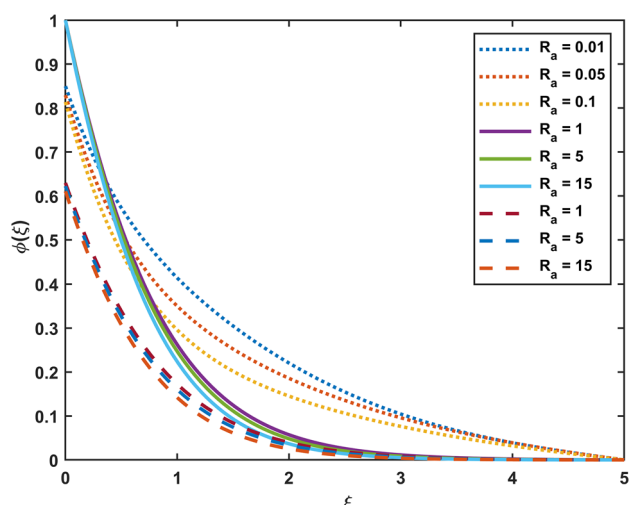


Table 2 is aimed to elucidate the values of C_f , Nu_x and Sh_x . It is apparent that increasing M , S_θ and S_ϕ decreases C_f , Nu_x and Sh_x , whilst on the contrary, the reverse trend is noticed for Gr and Gc . A rise in the values of s , Pr and Sc depreciates C_f which in turn enhances Nu_x and Sh_x , whereas the reverse phenomena is observed for β and S_v . As R , Ec , Q and R_a increases, C_f and Sh_x sky rockets but on the other hand, the heat transfer gets suppressed. Increasing the values of k declines Nu_x and C_f but the Sherwood number gets enhanced.

Fig. 14 Velocity profile for various k

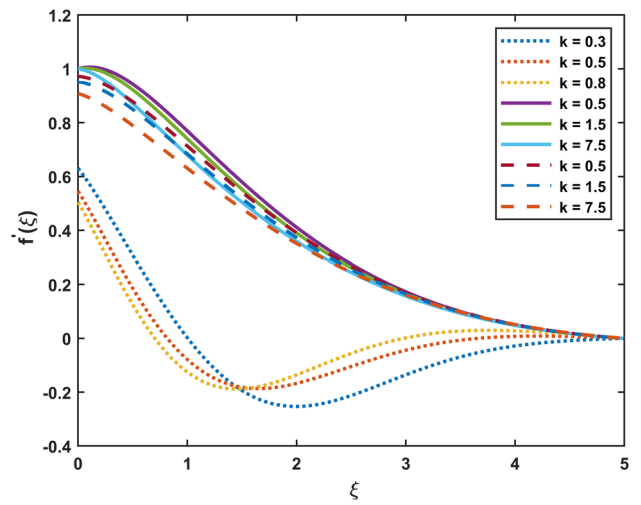


Fig. 15 Temperature distribution for various k

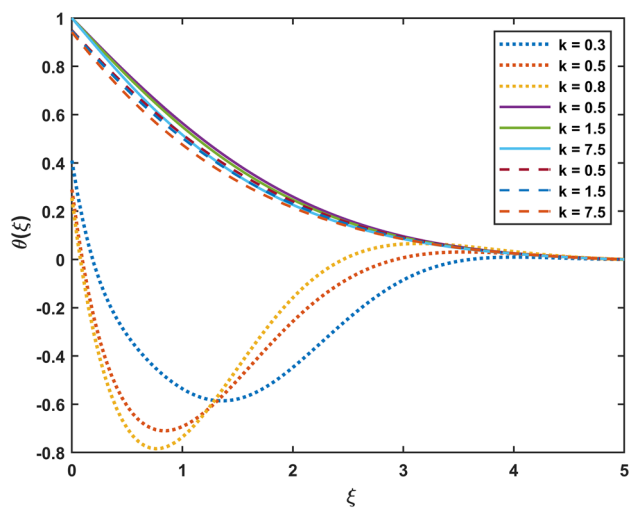


Fig. 16 Concentration distribution for various k

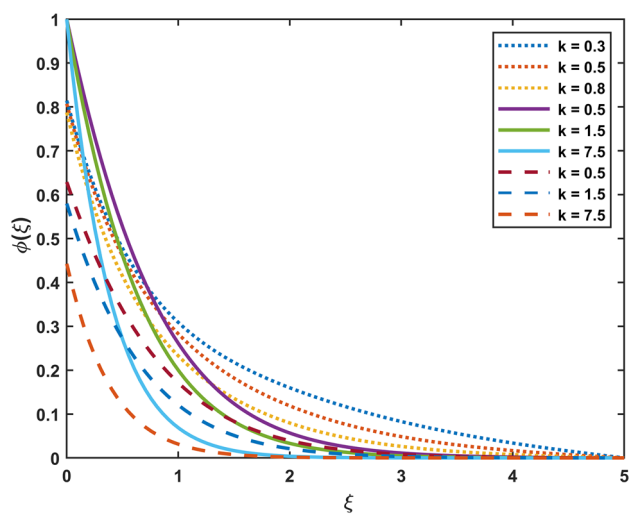


Fig. 17 Velocity profile for various s

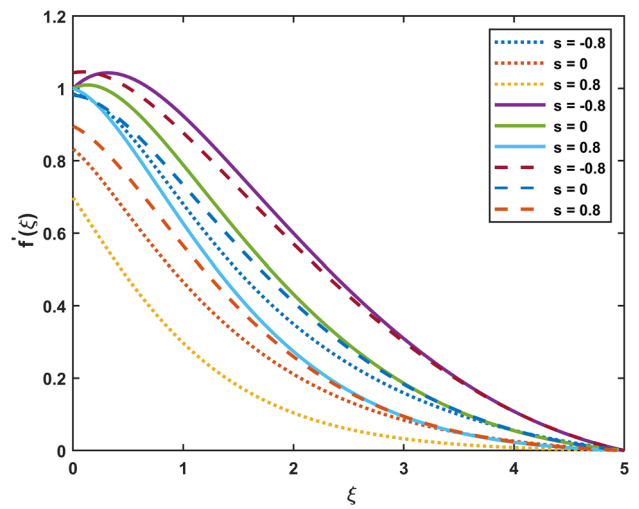


Fig. 18 Temperature distribution for various s

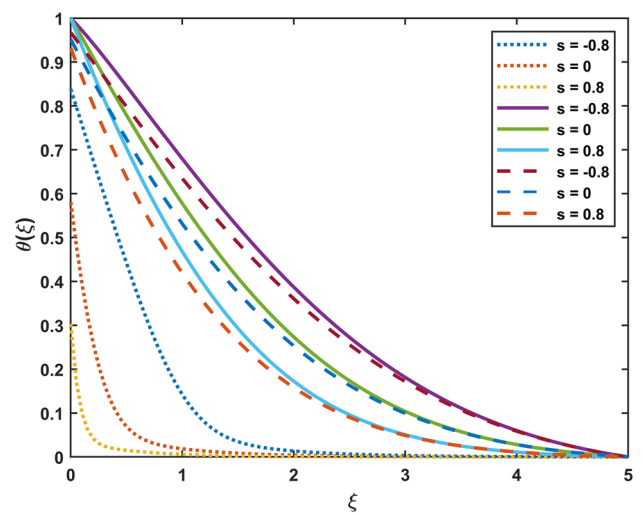


Fig. 19 Concentration distribution for various s

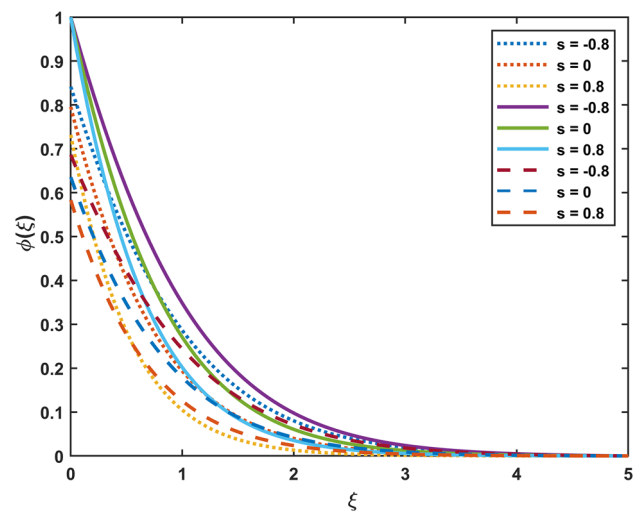


Fig. 20 Velocity profile for various S_v

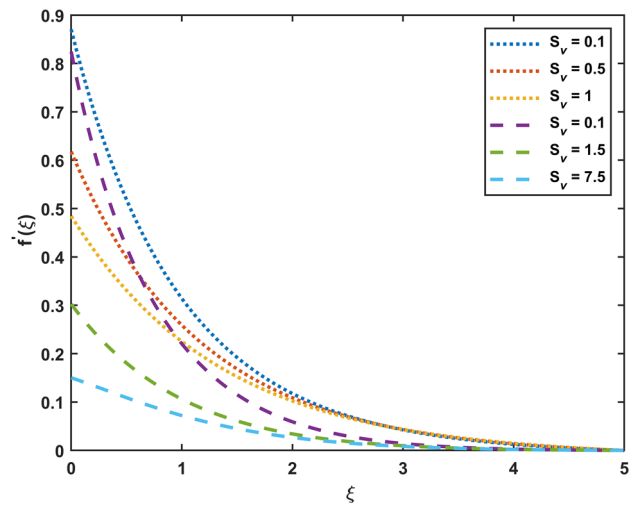


Fig. 21 Temperature distribution for various S_v

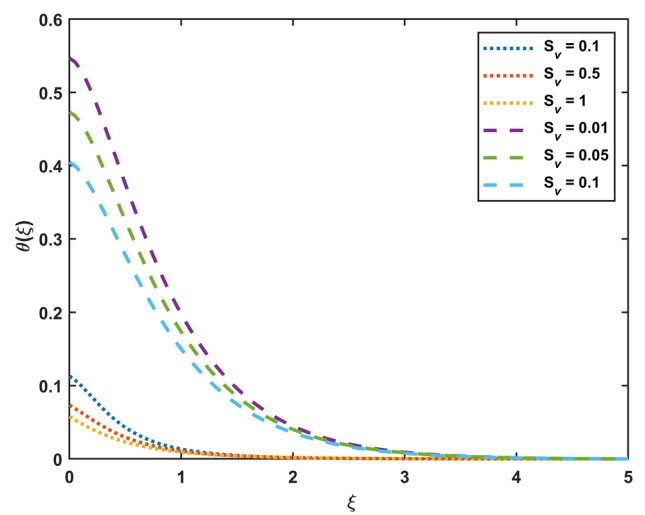


Fig. 22 Concentration distribution for various S_v

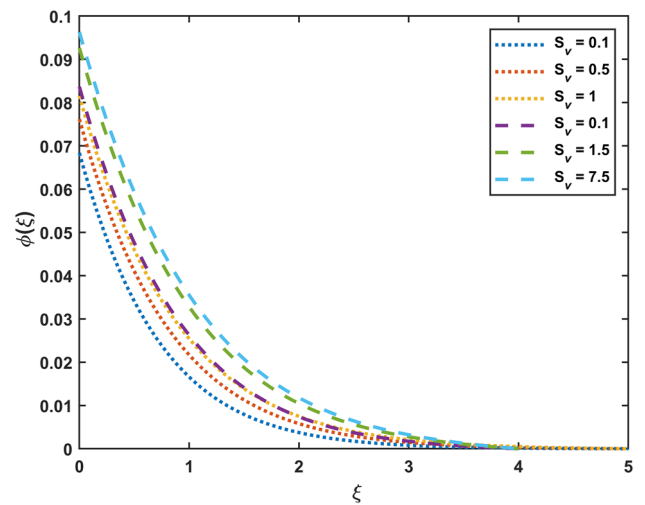


Fig. 23 Velocity profile for various S_θ

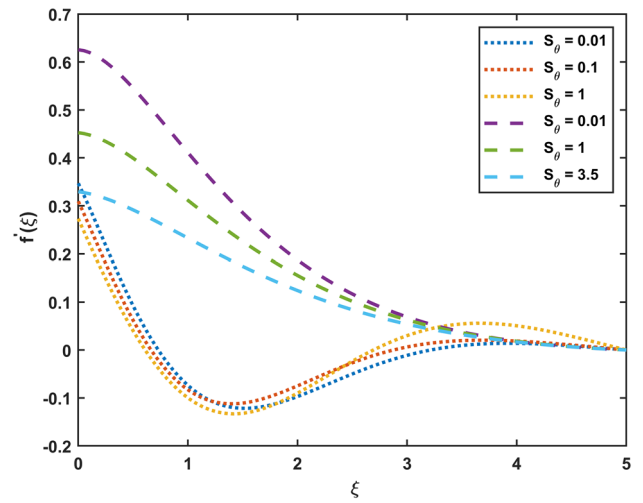


Fig. 24 Temperature distribution for various S_θ

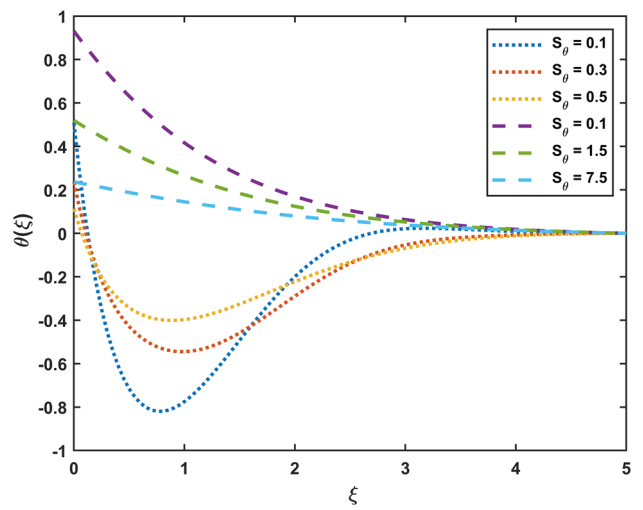


Fig. 25 Concentration distribution for various S_θ

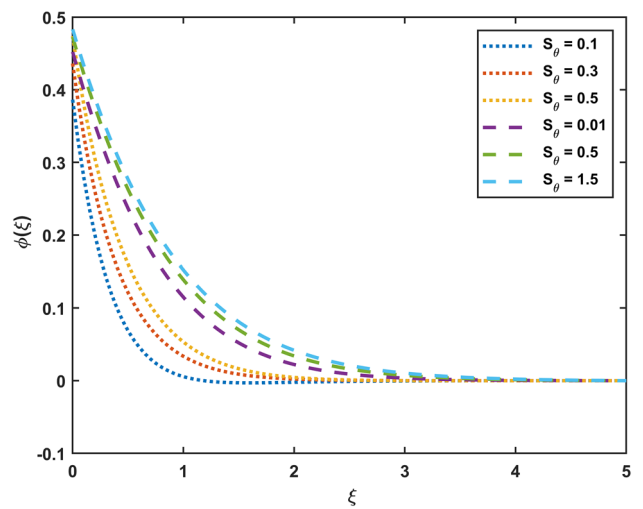


Fig. 26 Velocity profile for various S_ϕ

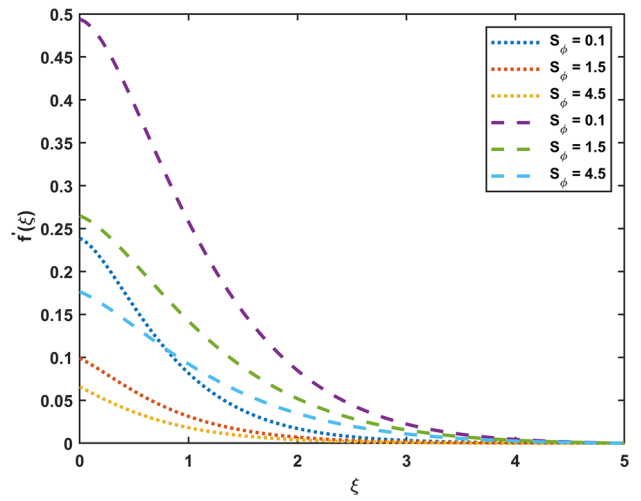


Fig. 27 Temperature distribution for various S_ϕ

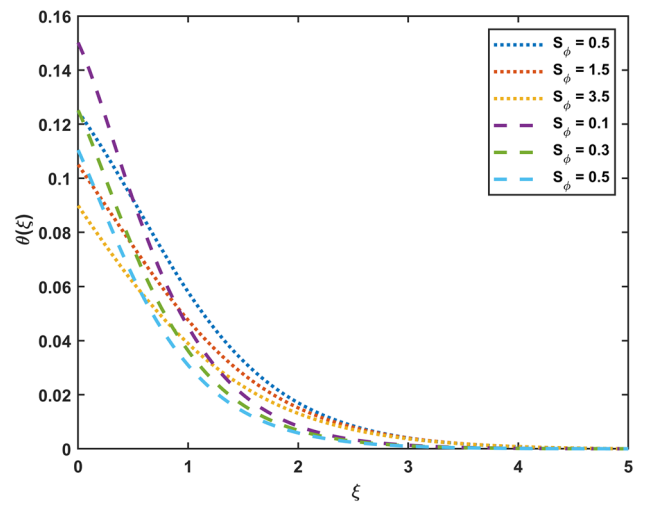


Fig. 28 Concentration distribution for various S_ϕ

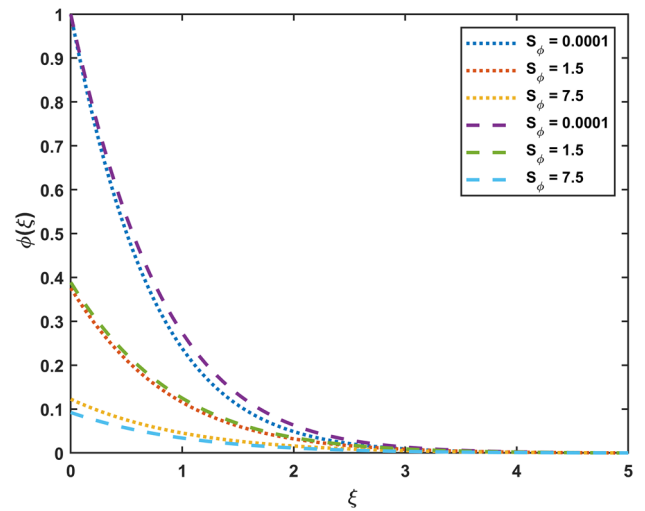


Fig. 29 Velocity profile for various β

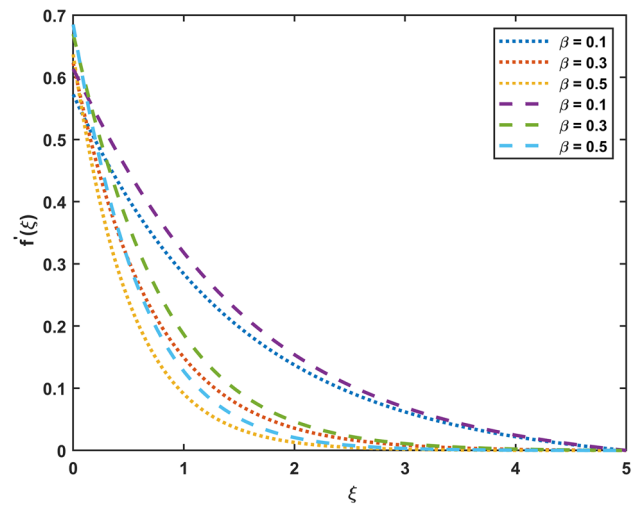


Fig. 30 Temperature distribution for various β

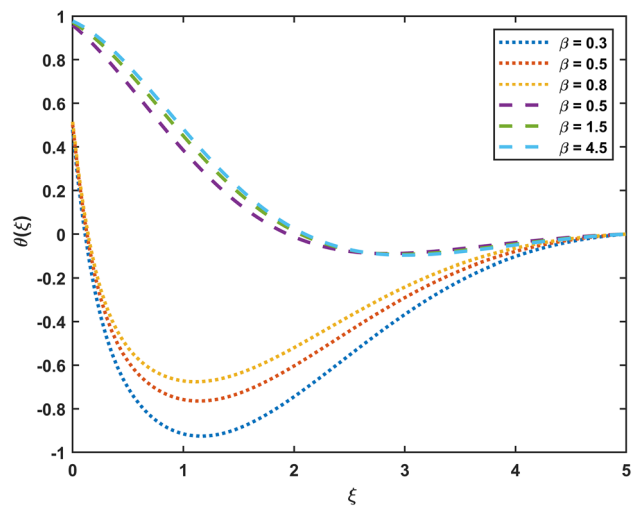


Fig. 31 Concentration distribution for various β

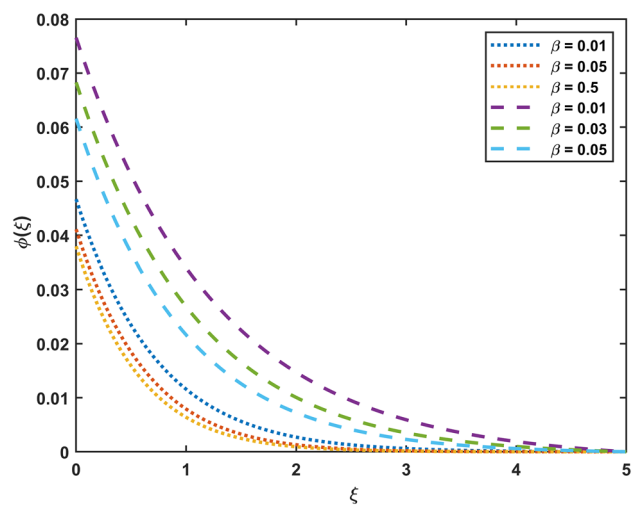


Table 2 Values of C_f , Nu_x and Sh_x for several values of pertinent parameters

| β | M | Gr | Gc | R | Ec | Q | Ra | k | S_v | S_θ | S_ϕ | s | Pr | Sc | $(1 + \frac{1}{\beta})f''(0)$ | $-\theta'(0)$ | $-\phi'(0)$ |
|---------|-----|------|------|-----|------|-----|------|-----|-------|------------|----------|-----|-------|------|-------------------------------|---------------|-------------|
| 2 | 0.5 | 0.5 | 0.5 | 0.5 | 0.1 | 0.5 | 0.1 | 0.5 | 0.2 | 0.2 | 0.2 | 0.5 | 0.7 | 0.7 | -0.659061 | 0.451921 | 0.929099 |
| 3 | | | | | | | | | | | | | | | -0.622405 | 0.450661 | 0.929078 |
| | 1 | | | | | | | | | | | | | | -0.859152 | 0.393257 | 0.906183 |
| | | 1 | | | | | | | | | | | | | -0.369847 | 0.512274 | 0.960041 |
| | | | 1 | | | | | | | | | | | | -0.461777 | 0.482027 | 0.947108 |
| | | | | 1 | | | | | | | | | | | -0.631917 | 0.381078 | 0.933857 |
| | | | | | 0.5 | | | | | | | | | | -0.638412 | 0.374694 | 0.932315 |
| | | | | | | 0.8 | | | | | | | | | -0.614341 | 0.315643 | 0.936489 |
| | | | | | | | 0.5 | | | | | | | | -0.639886 | 0.373097 | 0.931994 |
| | | | | | | | | 1 | | | | | | | -0.676245 | 0.449346 | 1.022371 |
| | | | | | | | | | 0.5 | | | | | | -0.429403 | 0.438169 | 0.915227 |
| | | | | | | | | | | 0.5 | | | | | -0.694680 | 0.386669 | 0.925002 |
| | | | | | | | | | | | 0.5 | | | | -0.704649 | 0.448973 | 0.723898 |
| | | | | | | | | | | | | 0.7 | | | -0.720218 | 0.488268 | 0.972126 |
| | | | | | | | | | | | | | 18.05 | 1.29 | -1.053517 | 2.526961 | 1.290290 |

6 Conclusion

In the present inspection, the reverberation of slip conditions jointly with the chemical reaction and radiation absorption across an exponentially stretching sheet of steady two-dimensional Casson fluid has been investigated. Until now no venture has been undertaken to scrutinize the effect of fluid flow for the case of ethyl alcohol, so it is considered in this article. The significant outcomes of the present analysis are:

- In the case of air, an enhancement in the radiation absorption parameter results in an elevation of the velocity profile and temperature distribution, whereas for ethyl alcohol, it is augmented close to the wall and suppressed at a distance farther from the wall in both circumstances.
- Monitoring the case of air, an upsurge of chemical reaction parameter skyrockets the Sherwood number, whilst opposite observation is perceived in the values of friction factor and Nusselt number.

Ethanol, an alcohol fuel, can be used to produce bio diesel. Furthermore, varying quantities of anhydrous ethanol is fused with petrol to minimize the consumption of petroleum fuels. In a hopeful manner, the results procured not merely furnishes valuable insights for applications, but additionally serves as a complement to the prior inquisitions.

Funding The author(s) received no financial support for the research, authorship, and/or publication of this article.

Data availability No Data associated in the manuscript.

Declarations

Conflict of interest The author(s) declare(s) no potential conflicts of interest with respect to the research, authorship, and/or publication of this article.

Appendix

Notation

- C_f Skin-friction coefficient
- C_w Wall concentration
- C_0 Reference concentration
- C_∞ Ambient concentration
- D_m Coefficient of mass diffusivity

| | |
|--------------|---|
| D_0 | Initial value of thermal slip factor |
| D_1 | Thermal slip |
| e_{ij} | $(i, j)^{\text{th}}$ component of deformation rate |
| Ec | Eckert number |
| E_0 | Initial value of solutal slip factor |
| E_1 | Solutal slip |
| g | Acceleration due to gravity |
| Gc | Concentration Grashof number |
| Gr | Thermal Grashof number |
| i, j | Particle index |
| k | Chemical reaction parameter |
| k^* | Mean absorption coefficient |
| L | Reference length |
| M | Magnetic field parameter |
| N_0 | Initial value of velocity slip factor |
| N_1 | Velocity slip |
| Nu_x | Nusselt number |
| Pr | Prandtl number |
| p_y | Yield stress |
| q_r | Radiative heat flux |
| Q | Heat source / sink parameter |
| R | Radiation parameter |
| R_a | Radiation absorption parameter |
| Re_x | Local Reynolds number |
| s | Suction/injection parameter |
| S_v | Velocity slip parameter |
| S_θ | Thermal slip parameter |
| S_ϕ | Solutal slip parameter |
| Sc | Schmidt number |
| Sh_x | Sherwood number |
| T_w | Temperature at the wall |
| T_0 | Reference temperature |
| T_∞ | Ambient temperature |
| U_0 | Initial stretching velocity |
| U | Velocity of the stretching surface |
| u, v | Velocity components in the x, y – directions respectively |
| β | Casson fluid parameter |
| β_C | Concentration expansion coefficient |
| β_T | Thermal expansion coefficient |
| κ | Thermal conductivity |
| μ | Dynamic viscosity |
| ν | Kinematic viscosity |
| ϕ | Dimensionless concentration |
| ρ | Density |
| (ρc_p) | Heat capacitance |
| σ | Electrical conductivity |
| σ^* | Stefan-Boltzmann constant |
| τ | Stress tensor |
| θ | Dimensionless temperature |

MATLAB code

MATLAB routine `bvp4c` can be executed by converting the boundary value problem (BVP) into initial value problem (IVP). Equations (11) to (15) take the form of the following simultaneous system of first ODE using linearity technique such as.

$$y_1 = f,$$

$$\begin{aligned}
 y_2 &= y_1' = f', \\
 y_3 &= y_2' = f'', \\
 y_4 &= \theta, \\
 y_5 &= y_4' = \theta', \\
 y_6 &= \varphi \text{ and} \\
 y_7 &= y_6' = \varphi'.
 \end{aligned}$$

Therefore,

$$\begin{aligned}
 y_3' &= \frac{1}{\left(1 + \frac{1}{\beta}\right)} (-y_1 y_3 + 2y_2 y_2 + M y_2 + 2Gc y_6 + 2Gr y_4), \\
 y_5' &= \frac{Pr}{\left(1 + \frac{4}{3}R\right)} \left(-y_1 y_5 + y_2 y_4 - Q y_4 - Ec \left(1 + \frac{1}{\beta}\right) y_3 y_3 - MEc y_2 y_2 - R_a y_6\right) \text{ and} \\
 y_7' &= Sc(y_2 y_6 - y_1 y_7) + kSc y_6,
 \end{aligned}$$

with the boundary conditions

$$y_1(0) = s, y_2(0) = 1 + S_v \left(1 + \frac{1}{\beta}\right) y_3(0), y_4(0) = 1 + S_\theta y_5(0), y_6(0) = 1 + S_\theta y_7(0), f'(\infty) \rightarrow 0, \theta(\infty) \rightarrow 0 \text{ and } \phi(\infty) \rightarrow 0$$

In order to solve (11)–(15) as an initial value problem, we need values for $f''(0)$, $\theta'(0)$ and $\phi'(0)$, but no such values are given prior to the computation. Thus, the initial guess values are chosen and the `bvp4c` method is applied to obtain the solution. We compared the calculated values at the far field boundary condition $\xi_\infty = \xi_{max} (= 5)$.

References

1. L.J. Crane, Flow past a stretching plate. *Zeitschrift für angewandte Mathematik und Physik ZAMP*. **21**(4), 645–647 (1970)
2. Casson N. A flow equation for pigment-oil suspensions of the printing ink type. *Rheol Disperse Syst.* (1959).
3. S. Mukhopadhyay, Slip effects on MHD boundary layer flow over an exponentially stretching sheet with suction/blowing and thermal radiation. *Ain Shams Eng. J.* **4**(3), 485–491 (2013)
4. S.J. Reddy, P. Valsamy, D.S. Reddy, Radiation and heat source/sink effects on MHD Casson fluid flow over a stretching sheet with slip conditions. *J. Math. Comput. Sci.* **11**(5), 6541–6556 (2021)
5. B.V. Swarnalathamma, D.P. Babu, M.V. Krishna, Combined impacts of radiation absorption and chemically reacting on MHD free convective casson fluid flow past an infinite vertical inclined porous plate. *J. Comput. Math. Data Sci.* **23**, 100069 (2022)
6. M.V. Krishna, Chemical reaction, heat absorption and Newtonian heating on MHD free convective Casson hybrid nanofluids past an infinite oscillating vertical porous plate. *Int. Commun. Heat Mass Trans.* **1**(138), 106327 (2022)
7. I.A. Shah, S. Bilal, S. Noeiaghdam, U. Fernandez-Gamiz, H. Shahzad, Thermosolutal natural convection energy transfer in magnetically influenced casson fluid flow in hexagonal enclosure with fillets. *Results Eng.* **1**(15), 100584 (2022)
8. J.V. Tawade, C.N. Guled, S. Noeiaghdam, U. Fernandez-Gamiz, V. Govindan, S. Balamuralitharan, Effects of thermophoresis and Brownian motion for thermal and chemically reacting Casson nanofluid flow over a linearly stretching sheet. *Results Eng.* **1**(15), 100448 (2022)
9. S.M. Mousavi, M.N. Rostami, M. Yousefi, S. Dinarvand, I. Pop, M.A. Sheremet, Dual solutions for Casson hybrid nanofluid flow due to a stretching/shrinking sheet: A new combination of theoretical and experimental models. *Chin. J. Phys.* **1**(71), 574–588 (2021)
10. N. Hameed, S. Noeiaghdam, W. Khan, B. Pimpunchat, U. Fernandez-Gamiz, M.S. Khan, A. Rehman, Analytical analysis of the magnetic field, heat generation and absorption, viscous dissipation on couple stress casson hybrid nano fluid over a nonlinear stretching surface. *Results Eng.* **1**(16), 100601 (2022)
11. J.A. Shercliff, *A Text Book of Magnetohydrodynamics* (Pergamon Press Inc., New York, 1965)
12. S. Pramanik, Casson fluid flow and heat transfer past an exponentially porous stretching surface in presence of thermal radiation. *Ain Shams Eng. J.* **5**(1), 205–212 (2014)
13. M.Q. Brewster, *Thermal Radiative Transfer and Properties* (John Wiley & Sons, New York, 1992)
14. L.F. Shampine, L.F. Shampine, I. Gladwell, S. Thompson, *Solving ODEs with matlab* (Cambridge University Press, Cambridge, 2003)

Springer Nature or its licensor (e.g. a society or other partner) holds exclusive rights to this article under a publishing agreement with the author(s) or other rightsholder(s); author self-archiving of the accepted manuscript version of this article is solely governed by the terms of such publishing agreement and applicable law.